Structural and Biochemical Consequences of Disease-Causing Mutations in the Ankyrin Repeat Domain of the Human TRPV4 Channel

Structural and biochemical consequences of disease-causing mutations in the ankyrin repeat domain of the human TRPV4 channel

Hitoshi Inada[†], *Erik Procko*[†,‡], *Marcos Sotomayor*[†,§], *and Rachelle Gaudet*[†,*]

[†]Department of Molecular and Cellular Biology, Harvard University, 52 Oxford Street, Cambridge, MA 02138

[‡]Present address: Howard Hughes Medical Institute and Department of Biochemistry, University of Washington, Seattle, WA 98195, USA

[§]Howard Hughes Medical Institute and Department of Neurobiology, Harvard Medical School, Boston, MA 02115, USA

AUTHOR EMAIL ADDRESS: gaudet@mcb.harvard.edu

TITLE RUNNING HEAD: Structural analysis of human TRPV4-ARD

CORRESPONDING AUTHOR FOOTNOTE: *To whom correspondence should be addressed: Rachelle Gaudet, Department of Molecular and Cellular Biology, Harvard University, 52 Oxford Street, Cambridge, MA 02138, USA, Tel.: (617) 495-5616; Fax: (617) 496-9684; E-mail: gaudet@mcb.harvard.edu

FOOTNOTES: This work was funded by NIH grant R01GM081340 to RG. This work is based upon research conducted at the Advanced Photon Source on the Northeastern Collaborative Access Team beamlines supported by award RR-15301 from the NCRR at the NIH. Advanced Photon Source is supported by the U.S. Department of Energy, Office of Basic Energy Sciences, under Contract No. DE-AC02-06CH11357. MS was an HHMI Fellow of the Helen Hay Whitney Foundation.

Keywords: human TRPV4; ankyrin repeat domain; inherited disease mutants

Abbreviations: ANK, ankyrin repeat; ARD, ankyrin repeat domain; ATP, adenosine triphosphate; CaM, calmodulin; CD, Circular dichroism; DTT, dithiothreitol; EDTA, ethylenediamine tetraacetic acid; HEPES, 4-(2-hydroxyethyl)-1-piperazineethanesulfonic acid; IPTG, isopropyl- β-D-thiogalactopyranoside; MD, molecular dynamics; PAGE, polyacrylamide gel electrophoresis; PDB, Protein Data Bank; PEG, polyethylene glycol; RMSD, Root-mean-square deviation; SDS, sodium dodecyl sulfate; SMD, steered molecular dynamics; TRP, transient receptor potential; TRPV, TRP vanilloid.

ABSTRACT

The TRPV4 calcium-permeable cation channel plays important physiological roles in osmosensation, mechanosensation, cell barrier formation, and bone homeostasis. Recent studies reported that mutations in TRPV4, including some in its ankyrin repeat domain (ARD), are associated with human inherited diseases including neuropathies and skeletal dysplasias, probably due to increased constitutive activity of the channel. TRPV4 activity is regulated by the binding of calmodulin and small molecules such as ATP to the ARD in its cytoplasmic N-terminus. We determined structures of ATP-free and -bound forms of human TRPV4-ARD and compared them with available TRPV-ARD structures. The third inter-repeat loop region (Finger 3 loop) is flexible and may act as a switch to regulate the channel activity. Comparisons of TRPV-ARD structures also suggest an evolutionary link between ARD structure and ATP binding ability. Thermal stability analyses and molecular dynamics (MD) simulations suggest that ATP increases stability in TRPV-ARDs that can bind ATP. Biochemical analyses of a large panel of TRPV4-ARD mutations associated with human inherited diseases showed that some impaired thermal stability while others reduced ATP binding ability, suggesting molecular mechanisms for the diseases.

Transient receptor potential (TRP) channels are cation channels involved in sensation of various stimuli from internal and external environments. The TRP channel superfamily is divided into six subfamilies in mammals: canonical or classical TRPC, vanilloid TRPV, melastatin TRPM, ankyrin TRPA, mucolipin TRPML, and polycystin TRPP.[1-3] Six TRPV proteins, TRPV1-6, belong to the vanilloid subfamily. TRPV proteins function as tetramers and each protomer contains six transmembrane segments flanked by two intracellular domains; a large N-terminal domain containing ankyrin repeats and a short C-terminal domain.

TRPV channel activity is regulated by post-translational modifications such as phosphorylation or binding of regulatory molecules to intracellular domains.[4, 5] In TRPV1, for example, ATP and calmodulin (CaM) have been shown to bind to the N-terminal ankyrin repeat domain (ARD) and sensitize or desensitize the channel activity, respectively.[6, 7] The binding of ATP and CaM to the ARD is also conserved in TRPV4 and TRPV3.[8] Phosphatidylinositol 4,5-bisphosphate (PIP_2) and CaM interact with the C-terminal domain of TRPV1 and regulate channel activity.[9-11] The molecular mechanisms by which these intracellular signals regulate TRPV channel activity remain unclear.

TRPV4 is a member of the TRPV subfamily expressed broadly in neuronal and non-neuronal cells. TRPV4 is activated by various stimuli including hypo-osmolarity, warm temperature, and chemical ligands such as 4-α-phorbol esters and epoxyeicosatrienoic acids.[12-15] Consistent with these *in vitro* findings, TRPV4 has been implicated in physiological functions such as osmoregulation and thermoregulation.[16, 17] TRPV4 also plays a role in mechanosensation in the vascular endothelium and unitary tract,[18] and cell barrier formation in vascular and epidermal tissues.[19] Recently, studies using TRPV4 knockout mice suggested the functional importance of TRPV4 in the central nervous system, nociception, and bone formation.[20-22]

Mutations in TRPV4 are associated with a wide spectrum of inherited diseases, primarily autosomal dominant neuropathies and skeletal dysplasias.[23, 24] Several mutants studied in heterologous expression systems showed constitutive basal activity and enhanced response to stimuli.[25-28] These findings are consistent with cell death caused by high calcium influx such as the observed degeneration of motor neurons in neuropathies.[27, 28] However, it is difficult to explain how seemingly similar molecular properties lead to such diverse disease phenotypes. It is therefore essential to elucidate how TRPV4 is regulated at the molecular level to understand the mechanisms behind these inherited diseases.

To obtain insight into regulatory mechanisms of TRPV4 we focused on the TRPV4-ARD, which can mediate channel regulation through binding of ligands to its concave surface and is the target of many mutations causing human diseases. We determined the structures of ATP-free and -bound human TRPV4-ARD and compared them with the structures of the other TRPV-ARDs. Despite a number of TRPV-ARD structures available either in the absence or presence of ATP, this represents the first cognate pair of ATP-free and -bound structures. Structural analysis revealed that a long loop forming Finger 3 is flexible and could switch conformation to possibly regulate channel activity. Comparisons of TRPV-ARD structures provide further insights into the evolution of ATP binding in TRPV channels. Thermal stability analyses, cysteine accessibility assay, and molecular dynamics (MD) simulations indicate that ATP binding can stabilize the TRPV1- and TRPV4-ARD. Interestingly, most mutations causing human genetic diseases in TRPV4-ARD are located away from the ATP-binding site, suggesting that additional regulatory interactions and mechanisms exist. A series of biochemical analyses of disease associated mutants showed that some impaired thermal

stability and/or ATP binding ability, providing biochemical insights about possible disease mechanisms.

EXPERIMENTAL PROCEDURES

Expression constructs. Human TRPV4 cDNA was obtained from Dr. Charlotte J. Sumner. The DNA fragment corresponding to the ARD (residues 149–396) was amplified by PCR and subcloned into the NdeI and NotI sites of a pET vector with a C-terminal six-histidine tag (pET21-C6H).[29] Mutations were generated with QuikChange (Stratagene) and confirmed by DNA sequencing.

Protein Production and Purification. Recombinant human TRPV4-ARD protein was expressed in *Escherichia coli* BL21(DE3) by induction with 75 μM isopropyl-β-D-thiogalactopyranoside for 13 hours at room temperature after the cells reached OD_{600} ~ 0.6. Frozen cell pellets were thawed, resuspended, and lysed by sonication in lysis buffer (20 mM Tris-HCl, 300 mM NaCl, 20 mM imidazole, pH 7.0) with 1 mM benzamidine, 1 mM phenylmethylsulfonyl fluoride (PMSF), 0.1% Triton X-100, 0.2 mg/ml lysozyme, 50 μg/ml RNase A, and 25 μg/ml DNase I. The lysate was cleared by centrifugation and the supernatant loaded onto nickel-nitrilotriacetic acid (Ni-NTA) agarose (Qiagen) and eluted by a step gradient containing 25, 50, 100, 150, 200, and 250 mM imidazole (pH 7.0) in lysis buffer with 0.05 % β-mercaptoethanol and 0.5 mM PMSF. Fractions containing the protein at 150, 200, and 250 mM imidazole were combined and EDTA (pH 8.0) was added to 1 mM final concentration, then dialyzed against 20 mM Tris-HCl (pH 7.0), 50 mM NaCl, 1 mM EDTA, and 1 mM DTT. The dialyzed protein was purified on SP Sepharose FF (GE Healthcare, Piscataway, NJ) in 20 mM Tris-HCl (pH 7.0), 1 mM EDTA, and 1 mM DTT using a linear gradient of 0 – 0.4 M NaCl. Size

exclusion chromatography on a Superdex 75 column (GE Healthcare, Piscataway, NJ) in 10 mM Tris-HCl (pH 7.0), 300 mM NaCl, 10 % glycerol, and 1 mM DTT was used for final purification. Protein was concentrated to ~8 mg/ml in a Vivaspin centrifugal filter (10,000 molecular weight cut off; Sartorius AG, Goettingen, Germany), flash frozen, and stored at –80°C. In the purification of mutant proteins for thermal stability assay, dialysis and ion exchange steps were omitted. After Ni-NTA purification, the proteins were purified by size exclusion chromatography in phosphate buffered saline (pH 7.4) with 1 mM DTT. Rat TRPV1-ARD (rTRPV1-ARD) was purified as described previously.[7]

Crystallization of human TRPV4-ARD. Crystals were grown by hanging-drop vapor diffusion at 4 °C: the ATP-free form with a ratio of 1:3 protein to reservoir solution (0.35 M NaH_2PO_4, 0.35 M KH_2PO_4, 10% glycerol, 0.1 M Na-HEPES pH 7.8); the ATP-bound form with a ratio of 1:1 protein to reservoir (3% PEG 4000, 10% glycerol, 0.1 M Na-HEPES pH 7.9) in the presence of 5 mM ATP. Crystals were soaked in reservoir solution containing 15% glucose for 3 min, then transferred into reservoir solution containing 30% glucose, and flash frozen in liquid nitrogen.

Data Collection, Structure Determination and Analysis. X-ray data were collected at 100 K using an ADSC Q315 detector at the Advanced Photon Source ID24 beamline, processed in HKL2000;[30] data statistics are listed in Table 1. The hTRPV4-ARD structures were determined by molecular replacement using the chicken TRPV4-ARD structure in MOLREP[31] and Phaser.[32] Model building was performed in COOT,[33] and refinement with TLS (Translation/Libration/Screw) in REFMAC5.[34] Final refinement statistics are listed in Table 1. The coordinates have been deposited in the Protein Data Bank with entry codes 4DX1 (ATP-free) and 4DX2 (ATP-bound). Figures were generated with PyMOL (Schrödinger, LLC.).

Thermal stability assay by circular dichroism spectroscopy. Circular dichroism (CD) spectra were measured at 10 ºC with 3.4 μM protein in 150 mM NaCl, 5 mM Tris-HCl, pH 7.5 and 1 mM DTT for experiments testing the influence of ATP on protein stability, and in phosphate buffered saline (pH 7.4) with 1 mM DTT for analyses of wild type and mutants. CD spectra were recorded in a 1 mm path length cuvette on a Jasco J-815 spectropolarimeter. For thermal stability, the molar ellipticity at λ = 222 nm was measured as the protein solutions were heated by 1 ºC/min, and used to determine the fraction of protein folded (assuming completely folded protein population at the starting temperature of 10 ºC). Thermal denaturation temperatures (T_m) were analyzed with Jasco Spectra software (JASCO Inc., Easton, MD), and listed ± standard deviation (SD).

Molecular dynamics simulation of rTRPV1-ARD. Two sets of molecular dynamics simulations (Apo and ATP) were carried out using the structure of rTRPV1-ARD bound to ATP, with or without the ATP ligand removed *in silico*, respectively (pdb code 2PNN, residues 111 to 356). Structures were solvated in explicit water (TIP3) and ions (100 mM NaCl) using VMD.[35] The systems contained 208,501 (ATP) and 208,482 (Apo) atoms. Minimization, equilibration, and steered molecular dynamics (SMD) simulations were performed in multiple steps using NAMD2.7,[36] CHARMM27 force field for proteins with the CMAP correction,[37, 38] full electrostatics, and 2-fs time steps with hydrogen bonds constrained. SMD simulations stretched both ends of TRPV1-ARD at an effective speed of 2 and 20 nm/ns.

ATP-Agarose Pulldown Assays. The ATP-agarose assays were performed as described previously.[28] Briefly, 20 μg of protein were incubated with 70 or 75 μl of 50% ATP agarose slurry for 1 hour at 4 °C in the binding buffer (10 mM Tris-HCl (pH 7.0), 50 mM NaCl, 1 mM DTT, and 0.15% n-decyl-D-maltopyranoside). After washing the agarose three times, proteins

were extracted and loaded on the 15% SDS gel. In each load lane, the volumes loaded corresponded to 1 μg of protein. Gels were quantified using ImageJ (National Institutes of Health, Bethesda, MD), and shown are the average ± SD for three independent experiments.

TRPV1 Cysteine Modification Assay. Reactions containing rTRPV1-ARD (8.5 μM) in 150 mM NaCl, 20 mM Tris (pH 7.0), 0.5 mM PEG-maleimide 5 kDa (Creative PEGWorks) and 10 mM nucleotide as indicated, were incubated at room temperature, stopped by addition of DTT to 110 mM, and analyzed by Coomassie-stained 12% SDS-PAGE.

Statistical Analyses. Statistical significance was tested by multiple comparisons using Tukey-Kramer or Dunnett's method with JMP software (SAS Institute Inc, Cary, NC).

RESULTS

Structures of Human TRPV4-ARD. Recombinant human TRPV4-ARD (hTRPV4-ARD, residues 149–396) produced in *E. coli* was purified for structure determination by X-ray crystallography and biochemical analyses. We determined the structure of hTRPV4-ARD in the absence (crystal form I; ATP-free) or presence (crystal form II) of ATP (Table 1). Both crystal forms contain two molecules per asymmetric unit. In crystal form II, one molecule is bound to ATP (ATP-bound) while the other is not (ATP-unbound). As expected based on previous structures of TRPV-ARDs,[7] hTRPV4-ARD consists of six ankyrin repeats (ANK1–6) each containing an inner and an outer helix followed by a connecting finger loop (Fingers 1–5) (Fig. 1A). The inner helices and fingers form a concave surface to which ATP is bound at the expected site previously identified in TRPV1.[7] Importantly, these structures represent the first cognate pair of ATP-bound and ATP-free TRPV-ARD structures.

The structures of hTRPV4-ARD were compared to each other and to those of chicken TRPV4-ARD (cTRPV4-ARD).[28] The structures of ATP-free hTRPV4-ARD and cTRPV4-ARD (residues 133-382, 90% sequence identity) are very similar (root mean squared deviation (RMSD) ranges from 0.635 to 0.922 Å over 239-242 Cα atoms) except at the tips of Fingers 2 and 3 (Fig. 1B). The same trend is apparent when extending this comparison to all ten available structures of TRPV4-ARD (four hTRPV4-ARD molecules in two crystal forms and six cTRPV4-ARD molecules in two crystal forms as well), with large structural differences observed in the very long Finger 3, as well as in the tip of Finger 2. Consistently, Finger 3 residues had high B-factors and were too disordered to trace in several cTRPV4-ARD structures, indicating high flexibility.

Structural Consequences of ATP Binding. Direct comparisons of the ATP-free and ATP-bound hTRPV4-ARD structures again show conformational differences restricted to Fingers 2 and 3 (Fig. 1A). Finger 3 was extended in ATP-free hTRPV4-ARD (and in ATP-free cTRPV4-ARD), while the finger loop was twisted and shrunken in ATP-bound hTRPV4-ARD. Finger 2 was also slightly twisted in ATP-bound hTRPV4-ARD. Surprisingly, both conformational differences were also observed when comparing the second, ATP-unbound, molecule in crystal form II to the ATP-free crystal form I structures (Fig. 1B). In crystal form II, an adjacent symmetry-related hTRPV4-ARD molecule occupied the ATP-binding site of the ATP-unbound molecule, possibly mimicking ATP binding. Alternatively, the shrunken Finger 3 structure may result from crystal contacts and/or crystallization condition differences.

One unusual feature of TRPV-ARDs is that many aromatic residues are exposed on the flexible Fingers 2 and 3.[29] In hTRPV4-ARD, nine of twenty aromatic residues are located on the

concave face of Fingers 2 and 3 (three and six residues, respectively; Fig. 2). Interestingly, F272 and F273 on Finger 3 are exposed in the ATP-free form, while these phenylalanines are buried in the shrunken Finger 3 of the ATP-bound form (Fig. 2B). The observed conformational differences may thus serve to regulate the exposure of the aromatic patch, and the conservation of the patch suggests that it is important, perhaps in interactions with regulatory ligands or with other regions of the full TRPV4 homotetramer.

Structural Comparison of TRPV-ARDs. Multiple TRPV-ARD structures are available: a structure of the rat TRPV1-ARD (rTRPV1-ARD) bound to ATP,[7] structures of cTRPV4-ARD in the absence of ATP, as well as structures of several ARDs that do not bind ATP, namely the rat and human TRPV2-ARDs and the mouse TRPV6-ARD[28, 39, 40] (see Table S1 of the Supporting Information). The overall structures of all available TRPV-ARDs are similar, with RMSD values ranging from 0.637 to 1.865 Å over 139-155 core Cα atoms (Table S2 of the Supporting Information). A superposition of all structures illustrates that the largest structural differences are again found in Fingers 2 and 3 (Fig. 3A). Structural comparisons of these TRPV-ARDs and the new human TRPV4-ARD highlight three noteworthy features.

First, as expected from biochemical, mutational and sequence analyses,[8] the interaction of ATP with the hTRPV4-ARD is very similar to what was previously observed in rTRPV1-ARD (Fig. 3B).[7] The adenine base fits in a conserved pocket, stacking against Tyr236 and hydrogen bonding to Gln239. Furthermore, Lys192 and Lys197 on the surface of inner helix 2 interact with the phosphate groups of ATP. These lysines are homologous to lysines critical for ATP binding in rTRPV1-ARD (Lys155 and Lys160)[7] and cTRPV4-ARD (Lys178 and Lys183).[8] The importance of Lys197 for ATP binding is further discussed below. The γ-phosphate of the ATP

is further removed from the protein in TRPV4 compared to TRPV1, consistent with the fact that the TRPV4-ARD showed less selectivity for ATP over ADP in ATP-agarose competition assays.[7]

Second, the backbone structure of ATP-bound hTRPV4-ARD, with a collapsed Finger 3, is quite similar to those of TRPV2-ARD and TRPV6-ARD, which lack the ability to bind ATP (Fig. 3C). In contrast, the ATP-free structures of chicken and human TRPV4-ARD, which both have the ability to bind ATP, have extended Finger 3 conformations (Fig. 1B and 3A). This visual observation is supported by comparing RMSD values for Fingers 2 and 3 of both ATP-free and -bound forms of hTRPV4-ARD with TRPV2-ARDs and mTRPV6-ARD: the ATP-bound form generally showed smaller RMSDs than the ATP-free form (Table S2 of the Supporting Information). This suggests that although the ARDs of TRPV2 and TRPV6 do not bind ATP, they are closest to the ATP-bound state of ARDs with ATP-binding sites, at least in structural terms.

Finally, the structure of ATP-bound hTRPV4-ARD and comparisons to TRPV2 and TRPV6 suggest that a previously unrecognized residue, Phe231 in hTRPV4-ARD, could be important for ATP binding. Phe231 is located under the adenine-stacking Tyr236 on Finger 2 (Fig. 3D), contributing to the adenine-binding pocket. This aromatic residue is conserved in the ATP-binding site of rTRPV1-ARD (Tyr194), while the aromatic residues are substituted with smaller aliphatic residues, cysteine or methionine, in TRPV2 and TRPV6 respectively (Fig. 3E). Sequence alignments of TRPV proteins confirm this trend, as the equivalent residue is a tyrosine in TRPV3, which binds ATP, and threonine in TRPV5, which does not. Substitution of these aromatic residues to cysteine (the residue found in the equivalent position in TRPV2) caused significant reduction of ATP binding in both rTRPV1-ARD and hTRPV4-ARD. In

rTRPV1-ARD, Y194C mutation reduced ATP binding comparably to K155A, identified in a previous study (Fig. 3F).[7] Significant reduction in ATP-binding was also observed in hTRPV4-ARD mutants F231C (Fig. 3G). These results indicate that the buried aromatic residue in Finger 2 conserved in TRPV1, TRPV3 and TRPV4 does indeed contribute to ATP binding in rTRPV1-ARD and hTRPV4-ARD.

ATP Binding Stabilizes TRPV4-ARD and TRPV1-ARD. ATP binding does not result in large conformational changes, but the ATP-bound form showed a tightly packed Finger 3 in both rTRPV1-ARD and hTRPV4-ARD structures, leading us to hypothesize that ATP may stabilize the proteins. In other ankyrin repeat proteins, such as IκBα and Notch, the ankyrin repeats are partially folded, and complete their folding as ligand is bound.[41-43] We therefore sought to determine whether ATP binding affected ARD stability. To this end, we analyzed the thermal stability of the hTRPV4-ARD by circular dichroism (CD) spectroscopy in the absence or presence of ATP, AMP or phosphate (Fig. 4). In buffer alone, hTRPV4-ARD showed a melting temperature (T_m) of 37.1 ± 0.1 °C. Phosphate ions (1 mM) increased T_m slightly but not significantly (37.33 ± 0.07 °C). In the presence of nucleotide ligands (1 mM), however, a small but significant increase in T_m was observed (T_m = 37.9 ± 0.2 for ATP and 37.4 ± 0.2 for AMP, respectively). The larger stabilization observed with ATP compared to AMP matches their differing binding affinity observed with cTRPV4-ARD.[8]

Stabilization of the ARD fold by nucleotides may also affect the accessibility of buried cysteine residues. hTRPV4-ARD contains four cysteines, two exposed (Cys194, Cys250) and two buried (Cys294, Cys353; Fig. S1). We examined the effect of ATP binding on ARD stability by measuring the kinetics of cysteine modification with PEG-maleimide (mPEG) in the

presence or absence of 10 mM AMP or ATP. hTRPV4-ARD was modified at endogenous cysteines by a 5 kDa PEG-maleimide, resulting in multiple shifted bands on SDS-PAGE. Furthermore, the rate of protein modification with mPEG was significantly reduced in the presence of nucleotides, especially ATP (Fig. S1). This suggests that the ARD fold is quite flexible, and that ATP binding stabilizes the fold, consistent with the thermal stability results described above.

To gain further insights into the effect of ATP binding on ARD stability, we used single cysteine mutants, allowing us to specifically address the accessibility of a buried cysteine. Interestingly, rTRPV1-ARD possesses a cysteine residue accessible to chemical modification by allicin, the active compound in garlic extract.[44] This cysteine residue, Cys157 (corresponding to Cys194 in hTRPV4-ARD), is paradoxically buried within the hydrophobic core of the TRPV1-ARD (Fig. 5A), suggesting that the structure may have some flexibility in solution, similar to that hypothesized for TRPV4-ARD above. Indeed, rTRPV1-ARD was modified at endogenous cysteines, similarly to hTRPV4-ARD, whereas no mobility shift was observed in a cysteine-less rTRPV1-ARD variant (CL) (Fig. 5B). More importantly, PEG-maleimide modification of a single-cysteine variant (C157) of rTRPV1-ARD, in which all cysteines except Cys157 were substituted with serine (C126S/C257S/C362S), resulted in a single shifted band (Fig. 5B). This result demonstrates that buried Cys157 is indeed accessible to modification (Fig. 5B), indicating a flexible and/or unstable fold. We hypothesized that ATP binding may stabilize the rTRPV1-ARD fold as it did hTRPV4-ARD. To test this hypothesis biochemically, we took advantage of the modifiable property of Cys157 to test the accessibility of this residue in the presence or absence of ATP. The single-cysteine variant rTRPV1-ARD CL-TRPV1-ARD C157 was chemically modified by PEG-maleimide with a half-time of 4 minutes ($t_{1/2}$ = 4 min) at

room temperature (Fig. 5C and 5D). Incubation with 10 mM ATP greatly inhibited the reaction, with $t_{1/2}$ = 52 min, consistent with ATP stabilizing the rTRPV1-ARD and limiting access to buried Cys157. In contrast, incubation with 10 mM ADP, a poor rTRPV1-ARD ligand,[7] only weakly inhibited Cys157 modification ($t_{1/2}$ = 10 min). CL-TRPV1-ARD C362, containing a single surface-exposed cysteine in the disordered C-terminal tail of the rTRPV1-ARD construct, was rapidly modified ($t_{1/2}$ < 30 seconds) even in the presence of nucleotides, confirming that ATP specifically inhibits the reaction of buried Cys157 (Fig. 5C and 5D). Therefore, as shown for hTRPV4-ARD above using CD spectroscopy, cysteine modification of hTRPV4-ARD and rTRPV1-ARD indicates that ATP binding can stabilize the TRPV-ARD fold.

To further confirm our results, we used steered molecular dynamics (SMD)[45] to pull the termini of TRPV1-ARD and reveal stable regions during protein mechanical unfolding *in silico*. The N- and C-termini were separated at a constant velocity of 2 nm/ns or 20 nm/ns in the presence or absence of bound ATP. TRPV1-ARD simulated in the absence of the bound ATP unfolded at both ends, with repeats 6 and then 1 unraveling during the time periods of independent simulations performed at either stretching speed (Fig. 5E and 5F). In contrast, when ATP, bound to repeats 1-3, was included in the simulations, repeat 6 and much of repeat 5 unravelled, while repeat 1 remained essentially intact (Fig. 5G and 5H). Unfolding forces were similar in the presence or absence of bound ATP at fast stretching speeds, but slightly larger for the ATP-bound ARD in the slower stretching simulations (Fig. S2 of the Supporting Information). These simulations therefore support the idea that ATP stabilizes the surrounding local TRPV1-ARD structure. Dynamic ligand-induced changes in TRPV-ARD stability may therefore provide a regulatory mechanism for channel sensitivity and activation.

Structural Analysis of TRPV4 Mutations Associated with Human Diseases. Many mutations in the TRPV4 gene have been associated with inherited diseases.[23, 24] Within the ARD, at least 15 mutations at 12 residues have been reported to cause autosomal dominant diseases classified either as neuropathies or skeletal dysplasias (Fig. 6A).[46-48] Mutations at arginine residues located on the convex face of hTRPV4-ARD are associated with neuropathies (Fig. 6B).[49] Arg232 and Arg269 are located on Finger 2 and 3, respectively, while Arg315 and Arg316 are located at the base of Finger 4. In contrast, eight residues whose mutations are associated with skeletal dysplasias - Glu183, Lys197, Leu199, Glu278, Thr295, Ile331, Asp333, and Val342 - are spread on both fingers and helices, primarily on the concave face of the hTRPV4-ARD (Fig. 2B). Therefore, mapping the available genetic data on the hTRPV4-ARD structure suggests that the phenotypic differences of the diseases may be related to differing functional properties of the concave and convex ARD surfaces.

To gain insights into possible biochemical mechanisms connecting the mutations with disease phenotype, we generated mutant hTRPV4-ARD corresponding to 13 of the 15 disease-causing mutations located within the ARD. We were not able to produce recombinant T295A hTRPV4-ARD because of its low protein expression and/or stability. The inability of T295A to fold stably when expressed in *E. coli* and the influence of nucleotide ligands on hTRPV4-ARD thermal stability suggest that several mutations could affect protein folding and/or stability. We therefore tested the thermal stability of wildtype hTRPV4-ARD and the 13 purified hTRPV4-ARD mutants by CD spectroscopy. Wildtype hTRPV4-ARD had a melting temperature (T_m) of 37.93 ± 0.08 °C (note that a phosphate-based buffer was used for these experiments). The T_m of most mutants was significantly different from wildtype, except for R232C and I331T (T_m = 38.1 ± 0.1 and 37.97 ± 0.07 °C, respectively; Table S4 and Fig. S3 of

the Supporting Information). Most mutations resulted in a significantly lower T_m, although R269C showed a significantly higher T_m (38.6 ± 0.2 °C) than wildtype (Table S4 of the Supporting Information). L199F and E183K showed the severest reductions in T_m (32.9 ± 0.1 °C and 33.78 ± 0.06, respectively). Leu199 is buried and tightly packed between inner helices 2 and 3 and therefore its substitution to a larger phenylalanine sidechain likely affects the protein thermal stability by disrupting the hydrophobic core packing arrangement (Fig. 6C). Glu183 is on the surface of Finger 2 and forms a salt bridge to Arg232 in some of the hTRPV4-ARD structures (Fig. 6D). However, simple disruption of this salt bridge is unlikely to cause this decrease in stability because the complementary R232C neutralizing mutation did not significantly alter the hTRPV4-ARD T_m. The E183K charge reversal may cause electrostatic repulsion between the ANK fingers due to proximity of Arg232, while the R232C mutation, disrupting the salt bridge, would not actively cause electrostatic repulsion. Overall, the averaged T_m of skeletal dysplasia mutants (35.6 ± 1.6 °C, n = 24) is significantly lower than those of wildtype (37.93 ± 0.08 °C, n = 8, p = 0.0005) and neuropathy mutants (36.9 ± 1.5 °C, n = 15, p = 0.017), although not all mutants obey this trend (Fig. 7A).

ATP Binding by hTRPV4-ARD Mutants. Most disease-associated mutations in TRPV4-ARD substitute surface-exposed sidechains. This suggests that interactions with other factors, such as other regions of the TRPV4 protein and/or regulatory ligands, are affected. Because ATP is a known ligand, we tested the ability of the hTRPV4-ARDs with disease-causing mutations to bind ATP using an ATP-agarose pulldown assay (Fig. 7B and 7C). Four mutants, K197R, R232C, R269H, and V342F, showed significantly reduced ATP binding. Lys197, which directly interacts with ATP in our ATP-bound hTRPV4-ARD structure (Fig. 3B), showed one of the greatest

reduction in ATP binding. This is also consistent with previously published experiments in which corresponding residues Lys183 of cTRPV4-ARD and Lys160 of rTRPV1-ARD were shown to be crucial for ATP binding.[7, 8] In contrast, the reduction in ATP binding observed for R232C and R269H is surprising because both residues are on the surface opposite to the ATP binding site (Fig. 6B). Similarly, ATP binding is significantly increased by the E183K and E278K mutations although these residues also have no direct interaction with ATP. These results suggest that, although the interaction of ATP is specific to the ATP-binding site observed in our structure,[8] it is influenced by the general electrostatic properties of the hTRPV4-ARD. Because intracellular ATP sensitizes TRPV4 channel activity,[8] enhanced ATP binding may result in higher activity of the channel, leading to constitutive basal activity. However, although several mutations either impaired or increased ATP binding, there was no correlation between the disease phenotypes and the ATP-binding phenotype.

In summary, increased ATP binding in E183K and E278K could contribute to the constitutive TRPV4 activity that is thought to lead to the TRPV4-linked disease phenotypes. However, it is difficult to explain the different disease phenotypes observed, including neuropathy and skeletal dysplasia, only based on changes in thermal stability or ATP binding (Fig. 7A and 7C), suggesting complex and unidentified mechanisms to regulate TRPV4 channel activity in different tissues.

DISCUSSION

In this study we determined the structures of ATP-free and -bound hTRPV4-ARD and compared them with the structures of other TRPV-ARDs. Structural analyses revealed the flexible Finger 3 as a possible switch to regulate channel activity. Biochemical analyses and MD

simulations indicated that ATP contributed to protein stability in TRPV-ARDs possessing ATP binding ability. Finally, a series of biochemical analyses of the disease-associated mutants showed that several have impaired thermal stability and/or ATP binding ability.

The new pair of crystal structures of the ATP-free and -bound forms of TRPV4-ARD revealed minimal conformational changes in the presence of bound ligand. The long and flexible Finger 3 undergoes the largest conformational change. In the process, a patch of aromatic residues is affected, such that a number of these aromatic residues are buried in the presence of ATP. This suggests that a regulatory signal could be exposed or hidden by a Finger 3 conformational change, to affect the sensitization of TRPV4 and the related TRPV1 channel by ATP.[7, 8] In other words, ATP binding may control the accessibility of a regulatory surface, which could interact intramolecularly with other parts of the TRPV4 channel or intermolecularly with additional regulatory factors. One candidate for such a regulatory factor is calmodulin, which was shown to require residues within the ATP binding site for binding to the TRPV4-ARD.[8]

It is interesting that the ATP-bound ARD structures of both TRPV1 and TRPV4, with their packed Finger 3, are similar to those of TRPV2 and TRPV6, which lack the ability to bind ATP. Although it does not bind ATP, in phylogenetic analyses TRPV2 clusters with TRPV1, TRPV3, and TRPV4, which can bind ATP. This clustering and the fact that most ATP-binding residues including two critical lysines are conserved in TRPV2[8] suggest that TRPV2 may have lost its ATP-binding ability in a relatively recent evolutionary process. A previous study attempted to generate a TRPV2-ARD mutant that could bind ATP and/or CaM by introducing two mutations: D78N, which neutralizes a negatively charged sidechain in close proximity to the phosphate interaction site, and H165Q, which could restore the adenine-binding pocket.[8] Although neither of the single mutants bound ATP, the double D78N/H165Q mutant bound ATP

weakly but significantly, suggesting that additional residues are essential for ATP binding. Our structure of ATP-bound TRPV4-ARD suggests a candidate: Phe231, which is conserved in the rTRPV1-ARD ATP binding site (Tyr194) but not in TRPV2 and TRPV6 (Fig. 3D). Comparing the TRPV-ARD structures suggests that this aromatic residue buttresses the adenine-binding pocket.

Several lines of evidence indicate that ATP binding increases protein stability of both TRPV1- and TRPV4-ARD (Fig. 4, 5, and S1). Interestingly, the TRPV4-ARD showed a T_m near body temperature (37.1 ± 0.1°C), suggesting that the ARD could be quite sensitive to changes in physiological temperature. In such a situation, a small but significant increase in T_m induced by binding of a ligand such as observed here for ATP (37.9 ± 0.2°C) may have large contribution to protein stability at body temperature. It has been reported that TRPV4 is activated by warm temperature (threshold for activation is ~34°C) and shows basal constitutive activity around body temperature.[13] Furthermore, it has been suggested that some unfolding event may be responsible for thermosensitivity of TRP channels.[50] Therefore, ARD stabilization by ligand binding may fine-tune TRPV4 function and basal activity levels, although the relationship between stability of ARD and channel activity remains speculative.

TRPV4 is unusual among the TRPV ion channels because a large number of dominant missense mutations have been identified that cause a whole spectrum of human skeletal dysplasias and neurodegenerative diseases. In particular, the neurodegenerative disease-causing mutations all localize to one surface of the ARD.[49] In contrast, the skeletal dysplasia mutations spread throughout the protein,[51] although a number of them are found in the ARD. We studied a total of 15 mutations at 12 positions localized to the ARD, five neurodegenerative disease mutations and 10 skeletal dysplasia mutations. Recently, two new mutations, Q239H (associated

with skeletal dysplasia, and located within the adenine pocket of the ATP-binding site) and R316H (associated with CMT2C like the previously identified R316C), have been reported in the ARD.[52,53] Several hTRPV4 mutants including both neurodegenerative mutations (R232C, R269C, R269H, R315W, and R316C) and skeletal dysplasia mutations (I331F and D333G) cause high basal activity and enhanced response to stimuli when expressed heterologously in HEK293 cells, and were inferred to cause cell death because of high Ca^{2+} influx.[26-28, 46, 53-55] The constitutive activity of hTRPV4 mutants is consistent with their dominant disease phenotypes. However, how different tissue-specific phenotypes are observed when both types of mutations result in a similar cellular phenotype remains unexplained.

We therefore generated 13 of the ARD mutant proteins and compared several of their biochemical properties. We did find several mutations causing significant enhancement or reduction in ARD thermal stability and/or ATP binding. These changes could participate in the disease mechanisms. Most hTRPV4-ARD mutants showed significantly reduced thermal stability, suggesting that the ARD thermal stability may contribute to the regulation of channel activity. For example, the ARD stability could alter the functional channel population as the TRPV4 N-terminus has been reported to be important for tetramer assembly.[56] However, a lower T_m does not provide a general correlation to TRPV4 function because R269C, which showed a higher T_m than wildtype, has been reported to cause the constitutive activity of the channel.[27, 28] Of note, the enhanced ATP binding by two skeletal dysplasia mutations, E183K and E278K, suggests a mechanism for increased TRPV4 activity and Ca^{2+} influx because intracellular ATP has been shown to sensitize TRPV4.[8]

Biochemical analyses in this study suggested two possible mechanisms for how mutations in TRPV4-ARD affect channel activity: reduced ARD thermal stability and increased

ATP binding. However, it is difficult to explain the disease-specific segregation based only on these two biochemical phenotypes, suggesting that additional mechanisms are likely at play to regulate TRPV4 channel. We also did not see a correlation between thermal stability and ATP binding, suggesting that there is no clear functional relationship between these two phenotypes. Our results therefore leave us with two broad hypotheses: (1) disease-causing TRPV4 mutations affect diverse regulatory mechanisms, converging to bone or neuron-related phenotypes in how they ultimately affect TRPV4 activity; or (2) the most important common mechanisms remain to be identified. That is, there could be regulatory factors or mechanisms specific to each tissue. Further understanding of the mechanisms which cause the human inherited diseases will therefore require the identification of tissue-specific biochemical phenotypes, as well as additional cell biology and electrophysiology studies to link biochemical findings to ion channel function.

ACKNOWLEDGEMENTS

We thank David Neau for assistance with data collection, Dr. Wilhelm A. Weihofen for help with data processing, Dr. Charlotte J. Sumner for providing human TRPV4 cDNA, Dr. Ute Hellmich for comments, and current and former lab members for technical help and discussions.

SUPPORTING INFORMATION

Table S1, TRPV-ARD structures used in this study; Table S2, Structural similarity between TRPV4-ARD and other TRPV-ARDs; Table S3, Molecular dynamics simulations of rat TRPV1-ARD; Table S4, T_m of wildtype and mutant TRPV4-ARD proteins; Figure S1, hTRPV4-ARD cysteine modification assay; Figure S2, Stability of TRPV1-ARD in equilibrium

and SMD simulations; Figure S3, Thermal stability of wildtype and mutant TRPV4-ARD proteins. This material is available free of charge via the Internet at http://pubs.acs.org.

REFERENCES

1. Clapham, D. E. (2003) TRP channels as cellular sensors, *Nature 426*, 517-524.

2. Clapham, D. E., Montell, C., Schultz, G., and Julius, D. (2003) International Union of Pharmacology. XLIII. Compendium of voltage-gated ion channels: transient receptor potential channels, *Pharmacol Rev 55*, 591-596.

3. Wu, L. J., Sweet, T. B., and Clapham, D. E. (2010) International Union of Basic and Clinical Pharmacology. LXXVI. Current progress in the mammalian TRP ion channel family, *Pharmacol Rev 62*, 381-404.

4. Tominaga, M., and Tominaga, T. (2005) Structure and function of TRPV1, *Pflugers Arch 451*, 143-150.

5. van de Graaf, S. F., Hoenderop, J. G., and Bindels, R. J. (2006) Regulation of TRPV5 and TRPV6 by associated proteins, *Am J Physiol Renal Physiol 290*, F1295-1302.

6. Rosenbaum, T., Gordon-Shaag, A., Munari, M., and Gordon, S. E. (2004) Ca2+/calmodulin modulates TRPV1 activation by capsaicin, *J Gen Physiol 123*, 53-62.

7. Lishko, P. V., Procko, E., Jin, X., Phelps, C. B., and Gaudet, R. (2007) The ankyrin repeats of TRPV1 bind multiple ligands and modulate channel sensitivity, *Neuron 54*, 905-918.

8. Phelps, C. B., Wang, R. R., Choo, S. S., and Gaudet, R. (2010) Differential regulation of TRPV1, TRPV3, and TRPV4 sensitivity through a conserved binding site on the ankyrin repeat domain, *J Biol Chem 285*, 731-740.

9. Prescott, E. D., and Julius, D. (2003) A modular PIP2 binding site as a determinant of capsaicin receptor sensitivity, *Science 300*, 1284-1288.

10. Ufret-Vincenty, C. A., Klein, R. M., Hua, L., Angueyra, J., and Gordon, S. E. (2011) Localization of the PIP2 sensor of TRPV1 ion channels, *J Biol Chem 286*, 9688-9698.

11. Numazaki, M., Tominaga, T., Takeuchi, K., Murayama, N., Toyooka, H., and Tominaga, M. (2003) Structural determinant of TRPV1 desensitization interacts with calmodulin, *Proc Natl Acad Sci U S A 100*, 8002-8006.

12. Liedtke, W., Choe, Y., Marti-Renom, M. A., Bell, A. M., Denis, C. S., Sali, A., Hudspeth, A. J., Friedman, J. M., and Heller, S. (2000) Vanilloid receptor-related osmotically activated channel (VR-OAC), a candidate vertebrate osmoreceptor, *Cell 103*, 525-535.

13. Guler, A. D., Lee, H., Iida, T., Shimizu, I., Tominaga, M., and Caterina, M. (2002) Heat-evoked activation of the ion channel, TRPV4, *J Neurosci 22*, 6408-6414.

14. Watanabe, H., Vriens, J., Suh, S. H., Benham, C. D., Droogmans, G., and Nilius, B. (2002) Heat-evoked activation of TRPV4 channels in a HEK293 cell expression system and in native mouse aorta endothelial cells, *J Biol Chem 277*, 47044-47051.

15. Watanabe, H., Vriens, J., Prenen, J., Droogmans, G., Voets, T., and Nilius, B. (2003) Anandamide and arachidonic acid use epoxyeicosatrienoic acids to activate TRPV4 channels, *Nature 424*, 434-438.

16. Liedtke, W. (2005) TRPV4 as osmosensor: a transgenic approach, *Pflugers Arch 451*, 176-180.

17. Tominaga, M., and Caterina, M. J. (2004) Thermosensation and pain, *J Neurobiol 61*, 3-12.

18. Mochizuki, T., Sokabe, T., Araki, I., Fujishita, K., Shibasaki, K., Uchida, K., Naruse, K., Koizumi, S., Takeda, M., and Tominaga, M. (2009) The TRPV4 cation channel mediates

stretch-evoked Ca2+ influx and ATP release in primary urothelial cell cultures, *J Biol Chem 284*, 21257-21264.

19. Sokabe, T., and Tominaga, M. (2010) The TRPV4 cation channel: A molecule linking skin temperature and barrier function, *Commun Integr Biol 3*, 619-621.

20. Shibasaki, K., Suzuki, M., Mizuno, A., and Tominaga, M. (2007) Effects of body temperature on neural activity in the hippocampus: regulation of resting membrane potentials by transient receptor potential vanilloid 4, *J Neurosci 27*, 1566-1575.

21. Alessandri-Haber, N., Dina, O. A., Joseph, E. K., Reichling, D., and Levine, J. D. (2006) A transient receptor potential vanilloid 4-dependent mechanism of hyperalgesia is engaged by concerted action of inflammatory mediators, *J Neurosci 26*, 3864-3874.

22. Masuyama, R., Vriens, J., Voets, T., Karashima, Y., Owsianik, G., Vennekens, R., Lieben, L., Torrekens, S., Moermans, K., Vanden Bosch, A., Bouillon, R., Nilius, B., and Carmeliet, G. (2008) TRPV4-mediated calcium influx regulates terminal differentiation of osteoclasts, *Cell Metab 8*, 257-265.

23. Nilius, B., and Owsianik, G. (2010) Transient receptor potential channelopathies, *Pflugers Arch 460*, 437-450.

24. Verma, P., Kumar, A., and Goswami, C. (2010) TRPV4-mediated channelopathies, *Channels (Austin) 4*, 319-328.

25. Rock, M. J., Prenen, J., Funari, V. A., Funari, T. L., Merriman, B., Nelson, S. F., Lachman, R. S., Wilcox, W. R., Reyno, S., Quadrelli, R., Vaglio, A., Owsianik, G., Janssens, A., Voets, T., Ikegawa, S., Nagai, T., Rimoin, D. L., Nilius, B., and Cohn, D. H. (2008) Gain-of-function mutations in TRPV4 cause autosomal dominant brachyolmia, *Nat Genet 40*, 999-1003.

26. Krakow, D., Vriens, J., Camacho, N., Luong, P., Deixler, H., Funari, T. L., Bacino, C. A., Irons, M. B., Holm, I. A., Sadler, L., Okenfuss, E. B., Janssens, A., Voets, T., Rimoin, D. L., Lachman, R. S., Nilius, B., and Cohn, D. H. (2009) Mutations in the gene encoding the calcium-permeable ion channel TRPV4 produce spondylometaphyseal dysplasia, Kozlowski type and metatropic dysplasia, *Am J Hum Genet 84*, 307-315.

27. Deng, H. X., Klein, C. J., Yan, J., Shi, Y., Wu, Y., Fecto, F., Yau, H. J., Yang, Y., Zhai, H., Siddique, N., Hedley-Whyte, E. T., Delong, R., Martina, M., Dyck, P. J., and Siddique, T. (2010) Scapuloperoneal spinal muscular atrophy and CMT2C are allelic disorders caused by alterations in TRPV4, *Nat Genet 42*, 165-169.

28. Landoure, G., Zdebik, A. A., Martinez, T. L., Burnett, B. G., Stanescu, H. C., Inada, H., Shi, Y., Taye, A. A., Kong, L., Munns, C. H., Choo, S. S., Phelps, C. B., Paudel, R., Houlden, H., Ludlow, C. L., Caterina, M. J., Gaudet, R., Kleta, R., Fischbeck, K. H., and Sumner, C. J. (2010) Mutations in TRPV4 cause Charcot-Marie-Tooth disease type 2C, *Nat Genet 42*, 170-174.

29. Jin, X., Touhey, J., and Gaudet, R. (2006) Structure of the N-terminal ankyrin repeat domain of the TRPV2 ion channel, *J Biol Chem 281*, 25006-25010.

30. Otwinowski, Z., and Minor, W. (1997) Processing of X-ray Diffraction Data Collected in Oscillation Mode, *Methods in Enzymology 276*.

31. Vagin, A., and Teplyakov, A. (2000) An approach to multi-copy search in molecular replacement, *Acta Crystallogr D Biol Crystallogr 56*, 1622-1624.

32. McCoy, A. J., Grosse-Kunstleve, R. W., Adams, P. D., Winn, M. D., Storoni, L. C., and Read, R. J. (2007) Phaser crystallographic software, *J Appl Crystallogr 40*, 658-674.

33. Emsley, P., and Cowtan, K. (2004) Coot: model-building tools for molecular graphics, *Acta Crystallogr D Biol Crystallogr 60*, 2126-2132.

34. Murshudov, G. N., Vagin, A. A., and Dodson, E. J. (1997) Refinement of macromolecular structures by the maximum-likelihood method, *Acta Crystallogr D Biol Crystallogr 53*, 240-255.

35. Humphrey, W., Dalke, A., and Schulten, K. (1996) VMD: visual molecular dynamics, *J Mol Graph 14*, 33-38, 27-38.

36. Phillips, J. C., Braun, R., Wang, W., Gumbart, J., Tajkhorshid, E., Villa, E., Chipot, C., Skeel, R. D., Kale, L., and Schulten, K. (2005) Scalable molecular dynamics with NAMD, *Journal of computational chemistry 26*, 1781-1802.

37. MacKerell, A. D., Jr. , Bashford, D., Bellott, M., Dunbrack, R. L., Jr., Evanseck, J. D., Field, M. J., Fischer, S., Gao, J., Guo, H., Ha, S., Joseph-McCarthy, D., Kuchnir, L., Kuczera, K., Lau, F. T. K., Mattos, C., Michnick, S., Ngo, T., Nguyen, D. T., Prodhom, B., Reiher, W. E., III., Roux, B., Schlenkrich, M., Smith, J. C., Stote, R., Straub, J., Watanabe, M., Wiórkiewicz-Kuczera, J., Yin, D., and Karplus, M. (1998) All-Atom Empirical Potential for Molecular Modeling and Dynamics Studies of Proteins, *J Phys Chem B 102*, 3586–3616.

38. Mackerell, A. D., Jr., Feig, M., and Brooks, C. L., 3rd. (2004) Extending the treatment of backbone energetics in protein force fields: limitations of gas-phase quantum mechanics in reproducing protein conformational distributions in molecular dynamics simulations, *J Comp Chem 25*, 1400-1415.

39. McCleverty, C. J., Koesema, E., Patapoutian, A., Lesley, S. A., and Kreusch, A. (2006) Crystal structure of the human TRPV2 channel ankyrin repeat domain, *Protein science : a publication of the Protein Society 15*, 2201-2206.

40. Phelps, C. B., Huang, R. J., Lishko, P. V., Wang, R. R., and Gaudet, R. (2008) Structural analyses of the ankyrin repeat domain of TRPV6 and related TRPV ion channels, *Biochemistry 47*, 2476-2484.

41. Croy, C. H., Bergqvist, S., Huxford, T., Ghosh, G., and Komives, E. A. (2004) Biophysical characterization of the free IkappaBalpha ankyrin repeat domain in solution, *Protein Sci 13*, 1767-1777.

42. Truhlar, S. M., Torpey, J. W., and Komives, E. A. (2006) Regions of IkappaBalpha that are critical for its inhibition of NF-kappaB.DNA interaction fold upon binding to NF-kappaB, *Proc Natl Acad Sci U S A 103*, 18951-18956.

43. Barrick, D., Ferreiro, D. U., and Komives, E. A. (2008) Folding landscapes of ankyrin repeat proteins: experiments meet theory, *Curr Opin Struct Biol 18*, 27-34.

44. Salazar, H., Llorente, I., Jara-Oseguera, A., Garcia-Villegas, R., Munari, M., Gordon, S. E., Islas, L. D., and Rosenbaum, T. (2008) A single N-terminal cysteine in TRPV1 determines activation by pungent compounds from onion and garlic, *Nat Neurosci 11*, 255-261.

45. Isralewitz, B., Gao, M., and Schulten, K. (2001) Steered molecular dynamics and mechanical functions of proteins, *Curr Opin Struct Biol 11*, 224-230.

46. Camacho, N., Krakow, D., Johnykutty, S., Katzman, P. J., Pepkowitz, S., Vriens, J., Nilius, B., Boyce, B. F., and Cohn, D. H. (2010) Dominant TRPV4 mutations in nonlethal and lethal metatropic dysplasia, *Am J Med Genet A 152A*, 1169-1177.

47. Dai, J., Kim, O. H., Cho, T. J., Schmidt-Rimpler, M., Tonoki, H., Takikawa, K., Haga, N., Miyoshi, K., Kitoh, H., Yoo, W. J., Choi, I. H., Song, H. R., Jin, D. K., Kim, H. T., Kamasaki, H., Bianchi, P., Grigelioniene, G., Nampoothiri, S., Minagawa, M., Miyagawa, S. I., Fukao, T., Marcelis, C., Jansweijer, M. C., Hennekam, R. C., Bedeschi, F., Mustonen, A., Jiang, Q., Ohashi, H., Furuichi, T., Unger, S., Zabel, B., Lausch, E., Superti-Furga, A., Nishimura, G., and Ikegawa, S. (2010) Novel and recurrent TRPV4 mutations and their association with distinct phenotypes within the TRPV4 dysplasia family, *J Med Genet 47*, 704-709.

48. Nishimura, G., Dai, J., Lausch, E., Unger, S., Megarbane, A., Kitoh, H., Kim, O. H., Cho, T. J., Bedeschi, F., Benedicenti, F., Mendoza-Londono, R., Silengo, M., Schmidt-Rimpler, M., Spranger, J., Zabel, B., Ikegawa, S., and Superti-Furga, A. (2010) Spondylo-epiphyseal dysplasia, Maroteaux type (pseudo-Morquio syndrome type 2), and parastremmatic dysplasia are caused by TRPV4 mutations, *American journal of medical genetics. Part A 152A*, 1443-1449.

49. Zimon, M., Baets, J., Auer-Grumbach, M., Berciano, J., Garcia, A., Lopez-Laso, E., Merlini, L., Hilton-Jones, D., McEntagart, M., Crosby, A. H., Barisic, N., Boltshauser, E., Shaw, C. E., Landoure, G., Ludlow, C. L., Gaudet, R., Houlden, H., Reilly, M. M., Fischbeck, K. H., Sumner, C. J., Timmerman, V., Jordanova, A., and Jonghe, P. D. (2010) Dominant mutations in the cation channel gene transient receptor potential vanilloid 4 cause an unusual spectrum of neuropathies, *Brain 133*, 1798-1809.

50. Clapham, D. E., and Miller, C. (2011) A thermodynamic framework for understanding temperature sensing by transient receptor potential (TRP) channels, *Proceedings of the National Academy of Sciences of the United States of America 108*, 19492-19497.

51. Dai, J., Cho, T. J., Unger, S., Lausch, E., Nishimura, G., Kim, O. H., Superti-Furga, A., and Ikegawa, S. (2010) TRPV4-pathy, a novel channelopathy affecting diverse systems, *J Hum Genet 55*, 400-402.

52. Andreucci, E., Aftimos, S., Alcausin, M., Haan, E., Hunter, W., Kannu, P., Kerr, B., McGillivray, G., Gardner, R. M., Patricelli, M. G., Sillence, D., Thompson, E., Zacharin, M., Zankl, A., Lamande, S. R., and Savarirayan, R. (2011) TRPV4 related skeletal dysplasias: a phenotypic spectrum highlighted byclinical, radiographic, and molecular studies in 21 new families, *Orphanet J Rare Dis 6*, 37.

53. Klein, C. J., Shi, Y., Fecto, F., Donaghy, M., Nicholson, G., McEntagart, M. E., Crosby, A. H., Wu, Y., Lou, H., McEvoy, K. M., Siddique, T., Deng, H. X., and Dyck, P. J. (2011) TRPV4 mutations and cytotoxic hypercalcemia in axonal Charcot-Marie-Tooth neuropathies, *Neurology 76*, 887-894.

54. Fecto, F., Shi, Y., Huda, R., Martina, M., Siddique, T., and Deng, H. X. (2011) Mutant TRPV4-mediated toxicity is linked to increased constitutive function in axonal neuropathies, *The Journal of biological chemistry 286*, 17281-17291.

55. Loukin, S., Su, Z., and Kung, C. (2011) Increased basal activity is a key determinant in the severity of human skeletal dysplasia caused by TRPV4 mutations, *PLoS One 6*, e19533.

56. Schaefer, M. (2005) Homo- and heteromeric assembly of TRP channel subunits, *Pflugers Arch 451*, 35-42.

FIGURE LEGENDS

Table 1. Data collection and refinement statistics

	Crystal form I (ATP free)	Crystal form II (with ATP)
Data collection		
Space group	$P3_121$	$P3_221$
Wavelength (Å)	0.97917	0.97917
Cell dimensions (a, b, c, Å)	53.30, 53.37, 440.71	147.89, 147.89, 93.90
Resolution (Å)[a]	40.0-2.85 (2.90-2.85)	40.0-2.95 (3.00-2.95)
R_{sym}[a]	0.115 (0.614)	0.099 (0.714)
$I/\sigma(I)$[a]	12.3 (1.8)	17.6 (2.4)
Completeness (%)[a]	99.6 (99.3)	100.0 (100.0)
Redundancy[a]	5.3. (5.4)	5.5 (5.6)
Refinement		
Resolution (Å)[a]	39.2-2.85 (2.92-2.85)	38.86-2.95 (3.03-2.95)
Number of reflections	17,306	23,958
R_{work}/R_{free}	0.215/0.278	0.177/0.220
Molecules/a. u.	2	2
Residues in model	148-397 (Chain A) 148-396 (Chain B)	148-394 (ATP-bound) 148-392 (ATP-unbound)
No. atoms		
Protein	1995 (Chain A) 1986 (Chain B)	1987 (ATP-bound) 1963 (ATP-unbound)
Ligand	25 (PO_4) 6 (Glycerol)	31 (ATP) 6 (Glycerol) 12 (Glucose)
Water	18	72
B-factors (Å)		
Protein	80.91	62.12 (ATP-bound) 72.76 (ATP-unbound)
Ligand	113.98 (PO_4) 103.44 (Glycerol)	91.00 (ATP) 72.51(Glycerol) 90.86 (Glucose)
Water	76.06	54.84
RMS deviations		
Bond lengths (Å)	0.013	0.013
Bond angles (deg)	1.51	1.80

[a] Values from the highest resolution are in parentheses.

Figure 1. Structural comparison of human and chicken TRPV4-ARDs. A, Superimposed ribbon diagrams of ATP-bound (magenta) and ATP-free (blue) hTRPV4-ARD. ATP is shown in stick representation. B, Superimposed Cα traces of human and chicken TRPV4-ARD. Finger 3 is twisted and shrunken in the ATP-bound (magenta) and -unbound (green) hTRPV4-ARD structures, while the finger is extended in ATP-free hTRPV4-ARD (blue) and cTRPV4-ARD (gray). Several Finger 3 residues are disordered in three of six TRPV4-ARD structures. The structure of Finger 2 in the ATP-bound and -unbound forms differs from ATP-free forms.

Figure 2. Aromatic residues on Fingers 2 and 3 vary their positions in hTRPV4-ARD structures. A, The hTRPV4-ARD structures of ATP-bound (magenta), ATP-unbound (green), and ATP-free (blue) forms are superimposed. Aromatic residues are shown as sticks. B, Detail of the Finger 2 and 3 loops. F272 and F273 on Finger 3 (indicated by black rectangles) are embedded in the aromatic cluster in the ATP-bound and -unbound forms, but exposed in the ATP-free form. Y235 and Y236 on Finger 2 and Y281 and F282 on Finger 3 are located in similar positions but show variable orientations. F231, F282, Y283, and F284 show less variation.

Figure 3. Structural comparison among TRPV-ARDs. A, Superimposed main chain structure of TRPV-ARDs (rTRPV1-ARD, gray; rat and human TRPV2-ARD, cyan; ATP-bound hTRPV4-ARD, magenta; ATP-unbound hTRPV4-ARD, green; ATP-free hTRPV4-ARD, blue; and mouse TRPV6-ARD, black). Finger 3 and a part of Finger 2 show high flexibility. Several residues on Finger 3 are missing in one of two TRPV1-ARD structures and four of seven TRPV2-ARD structures, respectively. B, ATP-binding site of hTRPV4-ARD and rTRPV1-ARD. Residues (sticks) within 4 Å of the ATP molecule and surface map of ATP binding site in

hTRPV4-ARD (left) and the corresponding residues in rTRPV1-ARD ATP binding site (right). Bound ATP molecule is shown as sticks (orange and yellow). C, Finger 2 (2) and Finger 3 (3) structures of ATP-bound rat TRPV1-ARD (gray), rat and human TRPV2-ARD (cyan), human ATP-bound TRPV4-ARD (magenta), and mouse TRPV6-ARD (black). D, An aromatic residue positioned behind the adenine base of ATP in Finger 2 (F231 in human TRPV4-ARD). E, This aromatic residue is conserved in TRPV-ARDs that bind ATP (red rectangle). F and G, ATP-agarose pulldown assays for wildtype and mutant rTRPV1-ARD (F) or hTRPV4-ARD (G). Coomassie-stained gels (top) of wildtype and mutant proteins loaded (left) and bound to ATP-agarose in the absence (middle) or presence (right) of competing free ATP. The normalized intensity of protein recovered (mean ± SD, n = 3) is plotted below. The statistical significance of the change in binding to ATP-agarose with respect to wildtype (WT) was determined by a multiple comparison test using Dunnett's method, with $p < 0.01$ indicated by *.

Figure 4. Effect of ATP on hTRPVh-ARD thermal stability. A, Representative circular dichroism spectra of the purified TRPV4-ARD protein (3.4 μM) in the presence of ATP, AMP, or phosphate (1mM each) at 10 ºC. The wavelength $\lambda = 222$ nm used for thermostability assays is indicated by a vertical red line. B, Representative traces of thermostability assay. The molar ellipticity at $\lambda = 222$ nm was measured as the protein solutions were heated by 1 ºC/min. C, T_m of TRPV4-ARD protein in the presence of 1 mM ATP, AMP, or phosphate. The statistical significance of the change in T_m was determined by a multiple comparison test using Tukey-Kramer method, with $p < 0.05$ and $p < 0.01$ indicated by * and **, respectively

Figure 5. ATP binding effect on protein stability in rTRPV1-ARD. A, The structure of TRPV1-ARD (grey) bound to ATP (green, sticks), with buried Cys157 highlighted (spheres). B, TRPV1-ARD is modified at cysteine residues by PEG-maleimide (mPEG), causing an electrophoretic mobility shift on a Coomassie-stained SDS-gel. WT, wildtype; CL, a cysteine-less variant; and C157, CL-TRPV1-ARD C157 single-cysteine variant. Shown is a representative Coomassie-stained gel from one out of three experiments. C, Time course for modification of single-cysteine TRPV1-ARD variants C157 and C362 with 0.5 mM mPEG at room temperature. D, Data from four experiments as in (C) were quantified and the mean ± standard deviation plotted. E and F, Molecular dynamics simulation in which the termini of the ATP-bound TRPV1-ARD (E) or TRPV1-ARD structure with ATP removed prior to equilibrating the system (F) are pulled apart at 20 nm/ns. Superimposed are the structures at the start (gold) and end (blue) of the simulations. G and H, The root mean square deviation of each Cα atom over the course of the simulation is mapped onto the starting models with (G) or without (H) ATP. Blue to red indicates 0 to 80 Å in RMSD. Simulations in which the termini were pulled apart at 2 nm/ns gave similar results. See Table S3 of the Supporting Information for experimental details.

Figure 6. Mutations associated with human diseases in the hTRPV4-ARD. A, Positions of mutations associated with human inherited diseases that lie within the hTRPV4-ARD. SEDM, spondyloepiphyseal dysplasia, type Maroteaux; SMDK, spondylometaphyseal dysplasia, type Kozolowski; MD, metatropic dysplasia; SMA, spinal muscular atrophy; SPMA, scapuloperoneal spinal muscular atrophy; CMTC2, Charcot-Marie-Tooth disease type 2C; HMSN2C, hereditary motor and sensory neuropathy 2C. This figure is inspired from ref [51]. B, Location of the diseases causing mutations within the TRPV4-ARD, shown as spheres are 12 residue positions at which a

total of 15 mutations causing human inherited diseases have been identified. The ATP molecule is shown as sticks. Skeletal dysplasia and neurophathy mutations are indicated as green and blue spheres, respectively. C, Leu199 is located in the hydrophobic interface between ANK2 and ANK3. D, Glu183 and Arg232 form a salt bridge on the convex face of the TRPV4-ARD.

Figure 7. Thermal stability and ATP binding of hTRPV4-ARD mutants associated with inherited diseases. A, The T_m determined by CD spectrometry in a phosphate-based buffer is plotted for wildtype and mutant hTRPV4-ARDs. The statistical significance is shown in Table S4 of the Supporting Information. B, Coomassie-stained gels show wildtype and mutant TRPV4-ARDs loaded (top) and bound to ATP-agarose (bottom). C, The normalized intensity of protein recovered (mean ± SD, n = 3). The statistical significance of the change in binding to ATP-agarose with respect to wildtype (WT) was determined by a multiple comparison test using Dunnett's method, with $p < 0.05$ and $p < 0.01$ indicated by * and **, respectively.

Figure 1

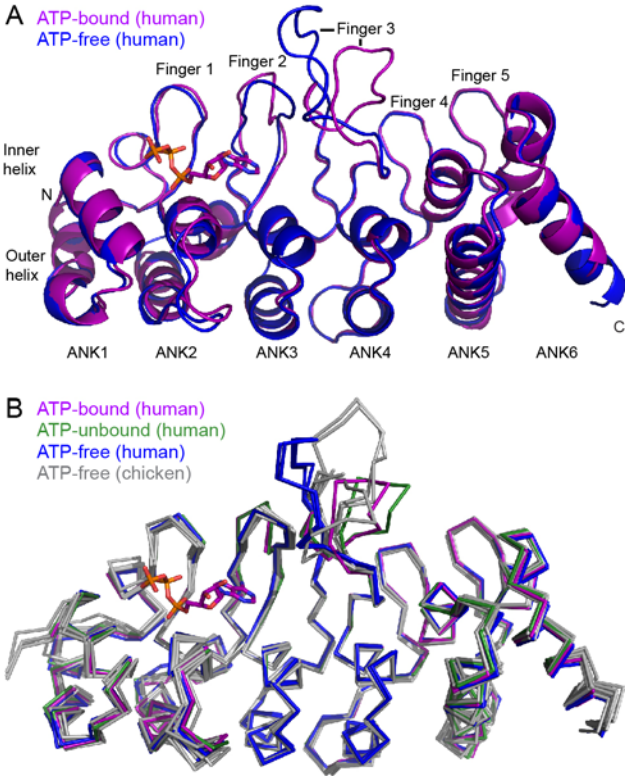
A
ATP-bound (human)
ATP-free (human)
Finger 1
Finger 2
Finger 3
Finger 4
Finger 5
Inner helix
N
Outer helix
C
ANK1
ANK2
ANK3
ANK4
ANK5
ANK6
B
ATP-bound (human)
ATP-unbound (human)
ATP-free (human)
ATP-free (chicken)

Figure 2

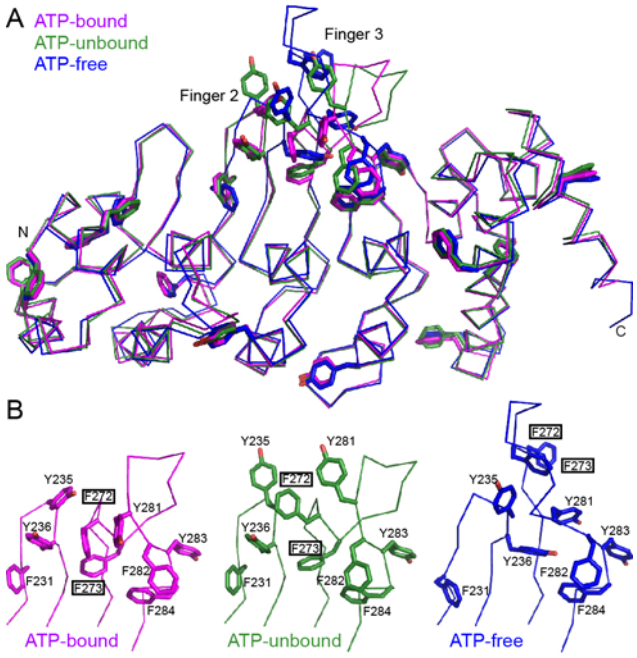
A
ATP-bound
ATP-unbound
ATP-free
Finger 3
Finger 2
N
C
B
Y235
F272
Y281
Y236
Y283
F231
F273
F282
F284
ATP-bound
ATP-unbound
ATP-free

Figure 3

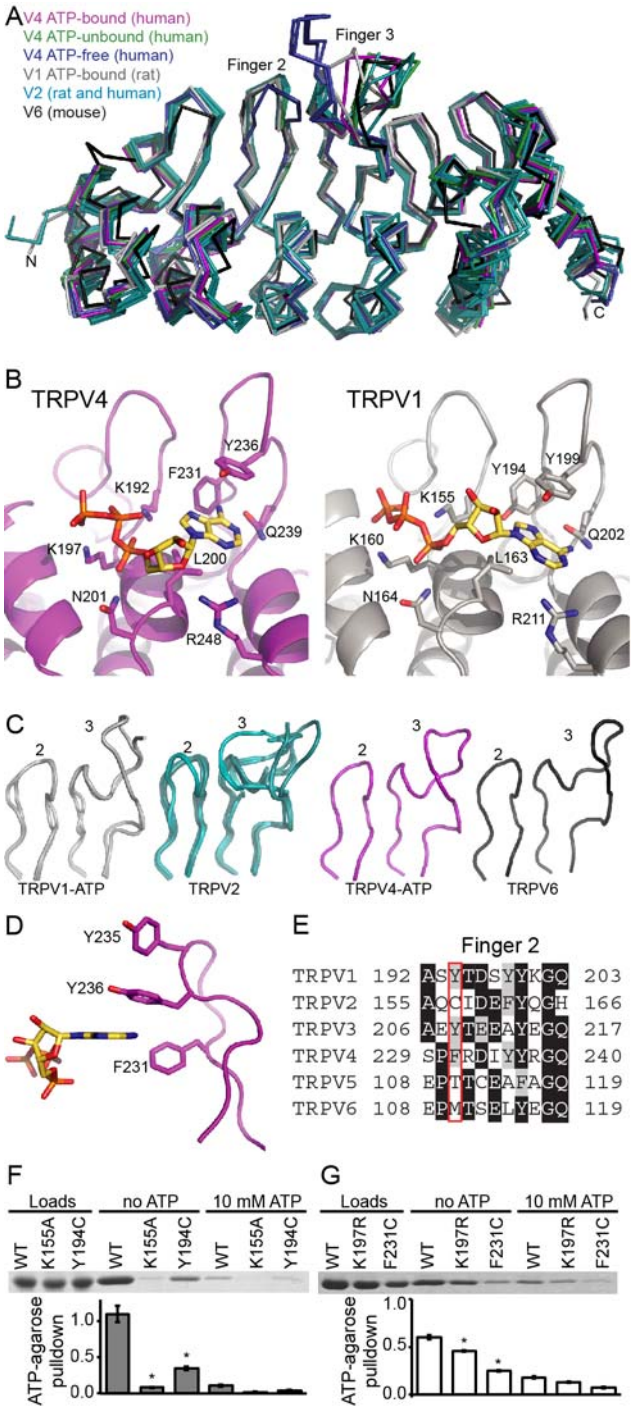
A
V4 ATP-bound (human)
V4 ATP-unbound (human)
V4 ATP-free (human)
V1 ATP-bound (rat)
V2 (rat and human)
V6 (mouse)
Finger 3
Finger 2
N
C
B
TRPV4
Y236
F231
K192
Q239
K197
L200
N201
R248
TRPV1
Y194
Y199
K155
K160
Q202
L163
N164
R211
C
TRPV1-ATP
TRPV2
TRPV4-ATP
TRPV6
D
Y235
Y236
F231
E
Finger 2
TRPV1 192 ASYTDSYYKGQ 203
TRPV2 155 AQCIDEFYQGH 166
TRPV3 206 AEYIEEAYEGQ 217
TRPV4 229 SPFRDIYYRGQ 240
TRPV5 108 EPTTCEAFAGQ 119
TRPV6 108 EPMTSELYEGQ 119
F
Loads
no ATP
10 mM ATP
WT
K155A
Y194C
ATP-agarose pulldown
G
Loads
no ATP
10 mM ATP
WT
K197R
F231C
ATP-agarose pulldown

Figure 4

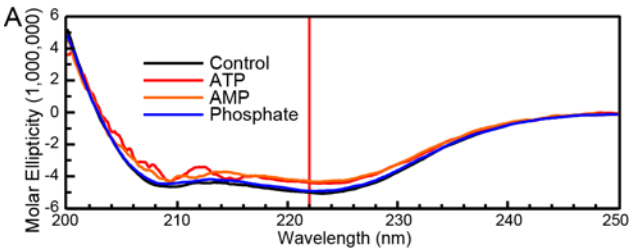

C

Condition	n	T_m ± SD (°C)
Control	4	37.1 ± 0.1
ATP	4	37.9 ± 0.2
AMP	4	37.4 ± 0.2
PO_4	4	37.33 ± 0.07

Figure 5

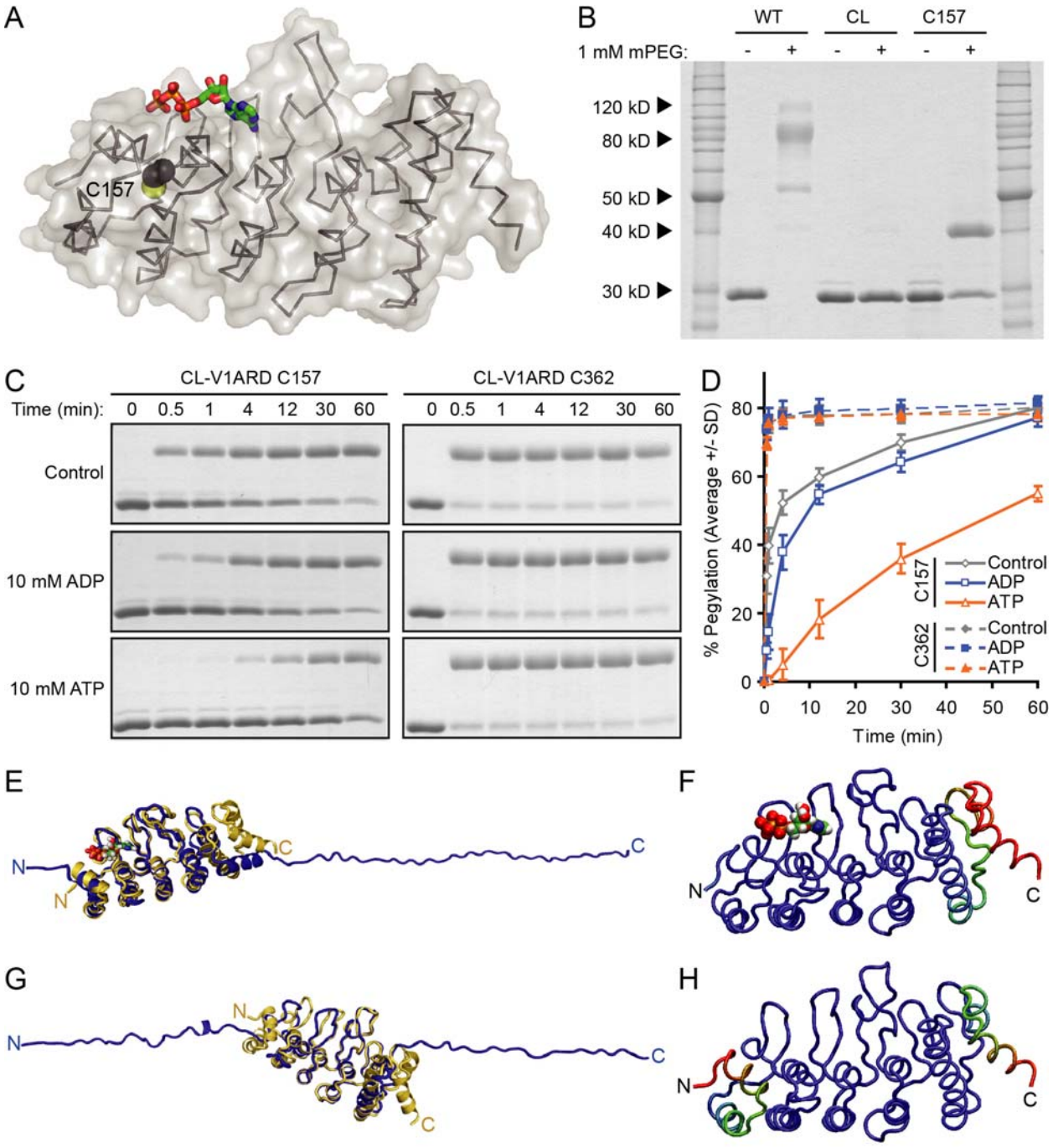
A
C157
B
WT
CL
C157
1 mM mPEG:
- + - + - +
120 kD
80 kD
50 kD
40 kD
30 kD
C
CL-V1ARD C157
CL-V1ARD C362
Time (min): 0 0.5 1 4 12 30 60
Control
10 mM ADP
10 mM ATP
D
% Pegylation (Average +/- SD)
Time (min)
C157
Control
ADP
ATP
C362
Control
ADP
ATP
E
N
C
N
C
F
N
C
G
N
C
N
C
H
N
C

Figure 6

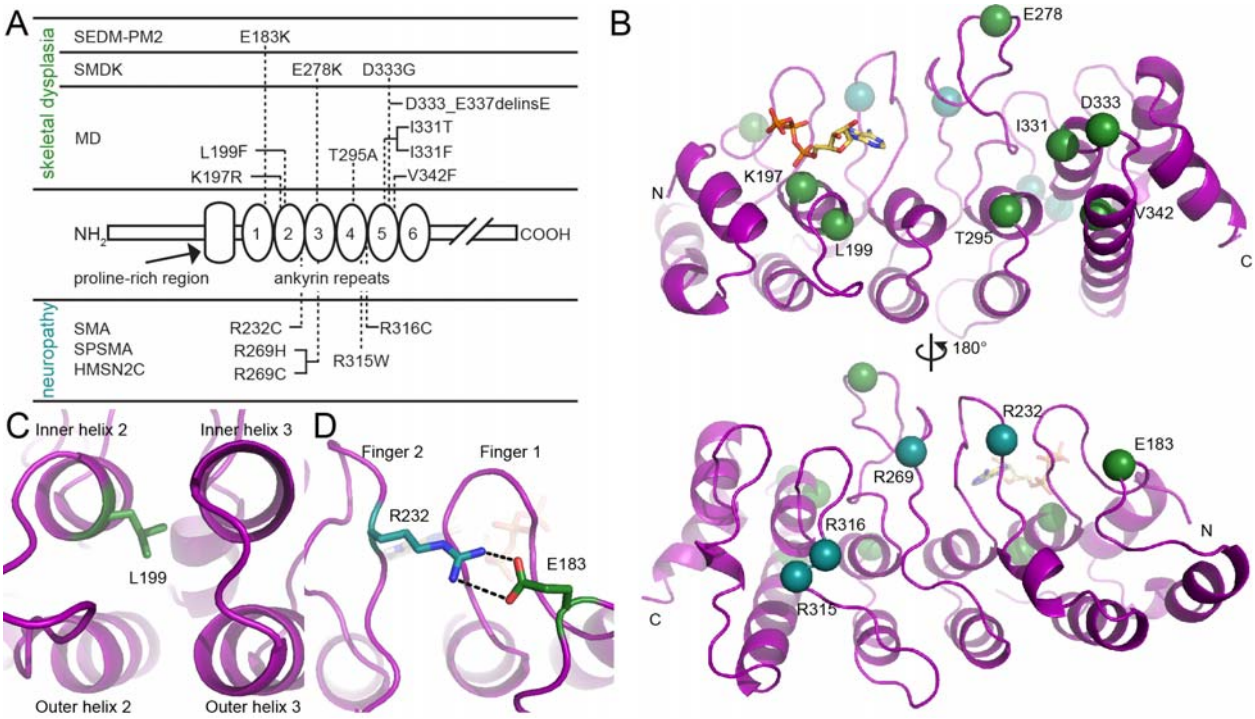
A
SEDM-PM2
E183K
SMDK
E278K
D333G
D333_E337delinsE
MD
I331T
L199F
T295A
I331F
K197R
V342F
skeletal dysplasia
NH2
1
2
3
4
5
6
COOH
proline-rich region
ankyrin repeats
neuropathy
SMA
SPSMA
HMSN2C
R232C
R269H
R269C
R315W
R316C
B
E278
D333
I331
K197
N
V342
T295
L199
C
180°
R232
E183
R269
R316
N
R315
C
C
Inner helix 2
Inner helix 3
L199
Outer helix 2
Outer helix 3
D
Finger 2
Finger 1
R232
E183

Figure 7

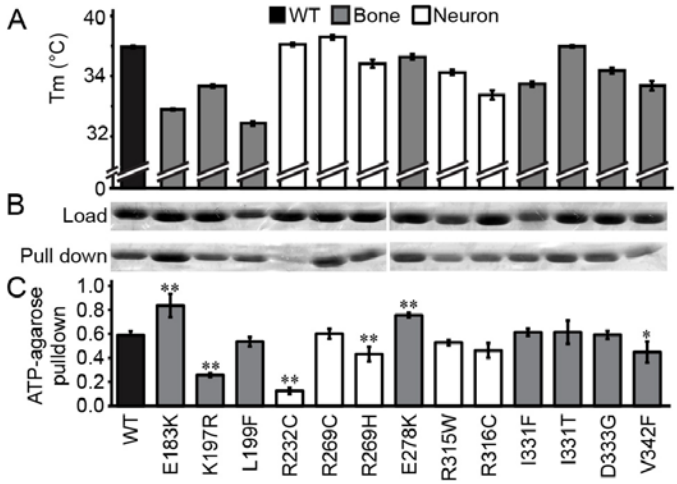
A
WT
Bone
Neuron
Tm (°C)
40
34
32
0
B
Load
Pull down
C
ATP-agarose pulldown
1.0
0.8
0.6
0.4
0.2
0.0
**
*
WT
E183K
K197R
L199F
R232C
R269C
R269H
E278K
R315W
R316C
I331F
I331T
D333G
V342F

For the Table of Contents Use Only

Structural and biochemical consequences of disease-causing mutations in the ankyrin repeat domain of the human TRPV4 channel

Hitoshi Inada, Erik Procko, Marcos Sotomayor, and Rachelle Gaudet

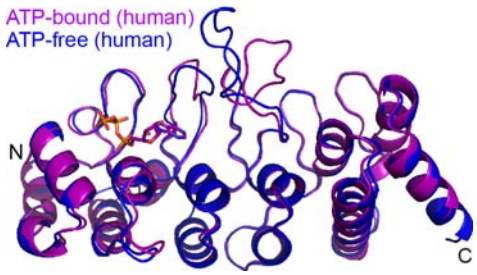

Structural and biochemical consequences of disease-causing mutations in the ankyrin repeat domain of the human TRPV4 channel

Hitoshi Inada, Erik Procko, Marcos Sotomayor, and Rachelle Gaudet

Supporting Information

Table S1. TRPV-ARD structures used in this study

Protein	Species	Structure (# mol/a.u.)	ATP binding	References
TRPV1	Rat	2PNN (1), 2NYJ (1)	+	Lishko *et al.,* 2007 (ATP-bound forms)
TRPV2	Rat	2ETA (2), 2ETB (1), 2ETC (2)	–	Jin *et al.,* 2006
	Human	2F37 (2)		McCleverty *et al.,* 2006
TRPV4	Human	Form I 4DX1 (2) without ATP	+	This study
		Form II 4DX2 (2) with 5 mM ATP		
	Chicken	3JXI (4), 3JXI (2)	+	Landouré *et al.,* 2010 (ATP-free forms)
TRPV6	Mouse	2RFA (1)	–	Phelps *et al.,* 2008

Table S2. Structural similarity between TRPV4-ARD and other TRPV-ARDs

TRPV	TRPV1	TRPV2			TRPV6	TRPV4	
Species	Rat	Rat		Human	Mouse	Chicken	
PDB	2PNN	2ETB	2ETC[a]	2F37[a]	2RFA	3JXI[a]	3JXJ[a]
RMSD[b]							
Finger 2[c]	1.596 / 0.279	1.527 / 0.245	1.251 / 1.081	1.577 / 0.227	1.538 / 0.259	0.183 / 1.599	0.213 / 1.617
Finger 3[d]	4.588 / 1.762	5.168 / 2.444	3.652 / 3.941	5.266 / 1.949	5.135 / 1.972	3.587 / 4.732	2.934 / 4.393
Core[e]	1.593 / 1.653	1.378 / 1.457	1.451 / 1.573	1.463 / 1.541	1.865 / 1.736	0.691 / 0.737	0.637 / 0.676

[a] Only the chains with complete loops were used in the analysis. [b] RMSD to human TRPV4-ARD (ATP-free, form I / ATP-bound, form II). [c] Residues 229-240 in hTRPV4. [d] Residues 261-287 in hTRPV4. [e] Residues 152-176, 194-228, 241-260, 288-307, 324-356, 373-394 in hTRPV4.

Table S3. Molecular dynamics simulations of rat TRPV1-ARD

Label	t_{sim} (ns)	Type[†]	Ensemble	SMD atoms	Speed (nm/ns)
	1.1[‡]	*EQ*	NpT	-	-
TRPV1-ARD-ATP	1.6	*SMD*	NVE	L111-Cα/H358-Cα	20
	8.3	*SMD*	NpT	L111-Cα/H358-Cα	2
	1.1[‡]	*EQ*	NpT	-	-
TRPV1-ARD-Apo	1.6	*SMD*	NVE	L111-Cα/H358-Cα	20
	8.3	*SMD*	NpT	L111-Cα/H358-Cα	2

[†] EQ denotes equilibrium simulations and SMD denotes constant velocity steered molecular dynamics.

[‡] These simulations consisted of 1,000 steps of minimization, 100 ps of dynamics with the backbone of the protein restrained (k = 1 kcal/mol/Å^2), and the remaining time as free dynamics in the NpT ensemble (Langevin damping set to 1 ps^{-1}).

Table S4. T_m of wildtype and mutant TRPV4-ARD proteins

Protein	N	Mean T_m	±	Std Dev (°C)	p-Value	
WT	8	37.93	±	0.08	1	
E183K	3	33.78	±	0.06	<.0001	*
K197R	3	35.3	±	0.1	<.0001	*
L199F	3	32.9	±	0.1	<.0001	*
R232C	3	38.1	±	0.1	0.8415	
R269C	3	38.6	±	0.2	<.0001	*
R269H	3	36.8	±	0.3	<.0001	*
E278K	3	37.3	±	0.2	<.0001	*
R315W	3	36.2	±	0.2	<.0001	*
R316C	3	34.7	±	0.3	<.0001	*
I331F	3	35.5	±	0.2	<.0001	*
I331T	3	37.97	±	0.07	1	
D333G	3	36.4	±	0.2	<.0001	*
V342F	3	35.4	±	0.3	<.0001	*

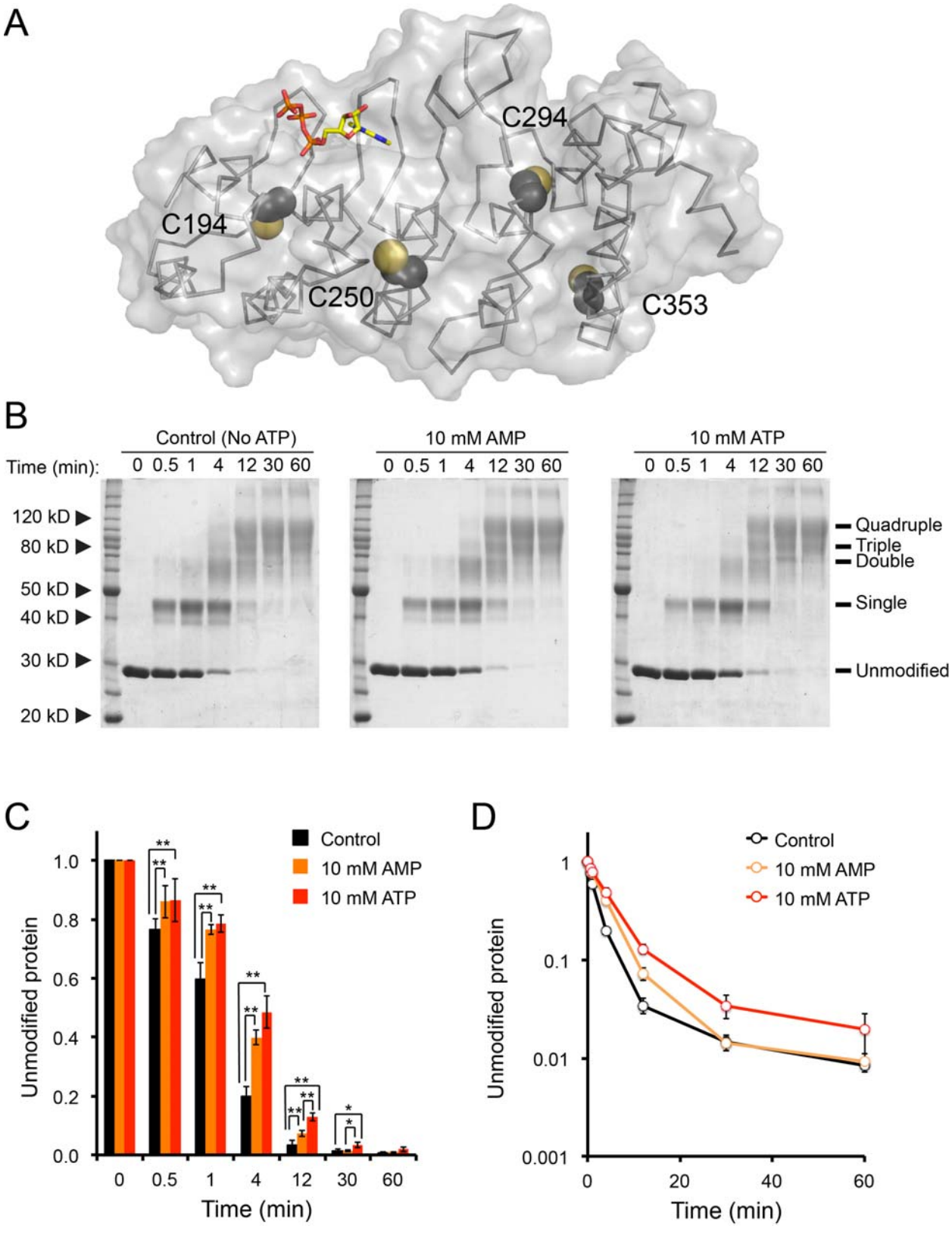
A
C294
C194
C250
C353
B
Control (No ATP)
10 mM AMP
10 mM ATP
Time (min):
0 0.5 1 4 12 30 60
120 kD
80 kD
50 kD
40 kD
30 kD
20 kD
Quadruple
Triple
Double
Single
Unmodified
C
Control
10 mM AMP
10 mM ATP
Unmodified protein
Time (min)
D
Control
10 mM AMP
10 mM ATP
Unmodified protein
Time (min)

Figure S1. ATP binding effect on protein folding/flexibility in hTRPV4-ARD. A, hTRPV4-ARD contains four cysteines (Cys194, Cys250, Cys294, and Cys353; spheres). Bound ATP is shown as yellow sticks. Cys194 corresponds to Cys157 in TRPV1, which is required for activation by chemical modification with allicin, a garlic extract compound.[1] B, Time course for modification of hTRPV4-ARD cysteines by PEG-maleimide (mPEG). Reactions containing hTRPV4-ARD (8.5 μM) in 150 mM NaCl, 20 mM Tris (pH 7.0), 0.5 mM mPEG-5 kDa (Creative PEGWorks) and 10 mM nucleotide as indicated, were incubated at room temperature, stopped by addition of DTT to 110 mM, and analyzed by Coomassie-stained 12% SDS-PAGE. hTRPV4-ARD modification at cysteine residues resulted in electrophoretic mobility shifts on a Coomassie-stained SDS-gel. Unmodified protein is reduced and modified proteins (single, double, triple, and quadruple) are increased in a time-dependent manner. Shown is a representative Coomassie-stained gel from one of three experiments. The statistical significance of the change in unmodified protein with respect to time point 0 was determined by a multiple comparison test using Tukey-Kramer method, with $p < 0.05$ and $p < 0.01$ indicated by * and **, respectively. C, Amount of unmodified protein in (B) is quantified as the mean ± standard deviation. D, Same data as in (C) with vertical axis in log scale.

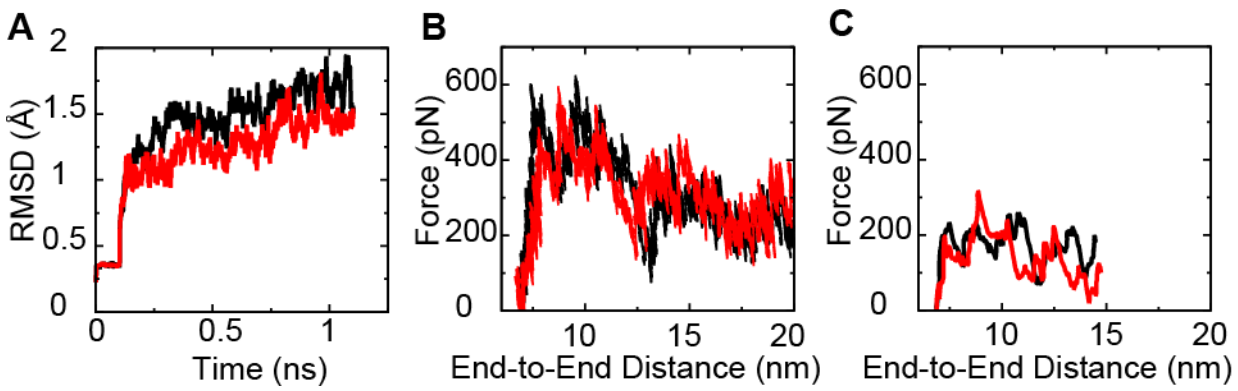

Figure S2. Stability of TRPV1-ARD in equilibrium and SMD simulations. A, Root mean square deviation (RMSD) is shown versus time during equilibrium simulations in the presence (red) and absence (black) of ATP. B and C, Force required to stretch and unfold TRPV1-ARD is shown as a function of the protein's end-to-end distance for simulations performed at 20 (B) and 2 nm/ns (C) with (red) and without (black) bound ATP.

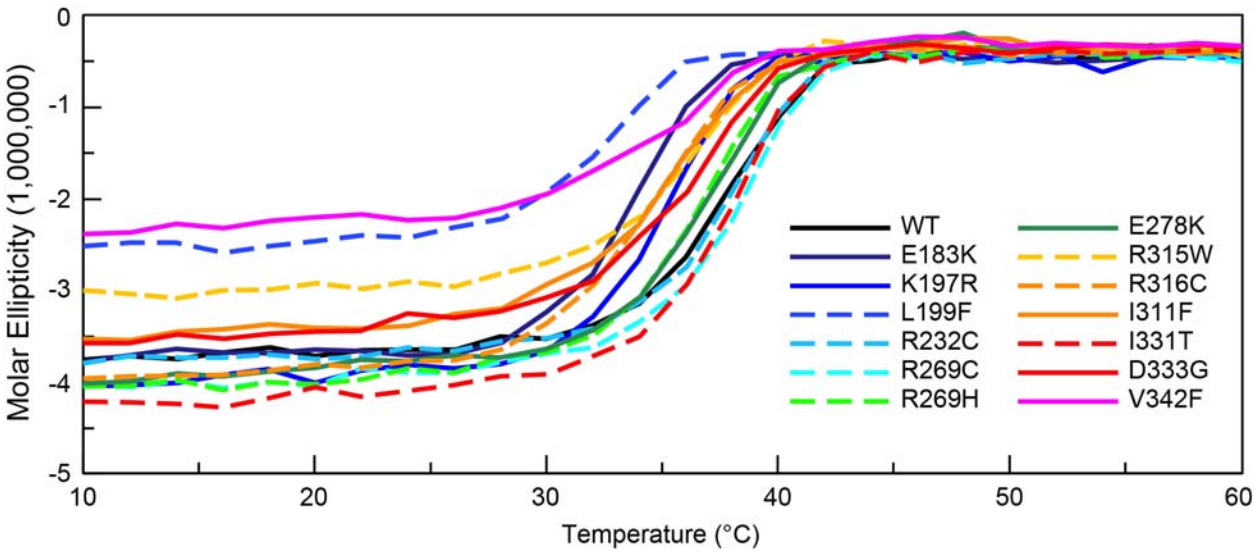

Figure S3. The thermal stability of wildtype and mutant TRPV4-ARD proteins. The molar ellipticity at $\lambda = 222$ nm was measured as the protein solutions were heated by 1 ºC/min.

Supplementary References

1. Salazar, H., Llorente, I., Jara-Oseguera, A., Garcia-Villegas, R., Munari, M., Gordon, S. E., Islas, L. D., and Rosenbaum, T. (2008) A single N-terminal cysteine in TRPV1 determines activation by pungent compounds from onion and garlic, *Nat Neurosci 11*, 255-261.